International Journal of Wildland Fire
doi: 10.1071/WF20153_AC

Supplementary material

Indications of positive feedbacks to flammability through fuel structure after high-severity fire in temperate eucalypt forests

Yogendra K. Karna[A,D], Trent D. Penman[A], Cristina Aponte[B], Cordula Gutekunst[C] and Lauren T. Bennett[A]

[A]School of Ecosystem and Forest Sciences, The University of Melbourne, 4 Water Street, Creswick, Vic. 3363, Australia.

[B]School of Ecosystem and Forest Sciences, The University of Melbourne, 500 Yarra Boulevard, Richmond, Vic. 3121, Australia.

[C]School of Landscape Ecology, University of Rostock, Justus-von-Liebig-Weg 6, 18059 Rostock, Germany.

[D]Corresponding author. Email: karnayogendra@gmail.com

Table S1: Lidar acquisition and sensor specifications from pre-fire and post-fire datasets.

Attribute	Pre-fire	Post-fire
Acquisition date	19 Nov 2007 - 10 Jan 2008	09 Jan–06 Aug 2016
Sensor type	ALTM3100EA	Trimble AX60
Flight altitude (m asl)	1300	800
Beam divergence (mrad)	Dual 0.3 & 0.8	≤ 0.25
Footprint (m)	0.26	0.22
Scan Rate (Hz)	71000	134
Swath (side) Overlap (%)	25	50
Maximum scan angle (^{0})	± 25	60 (FOV)
Average pulse spacing (m)	0.95	0.29
Average point density (m^{-2}) [a]	1.92	24.34
Horizontal Accuracy (cm)	± 35	≤20
Vertical Accuracy (cm)	± 50	≤20
Stored Data Format	LAS v1.0	LAS v1.3
Tile size	2km*2km	1km * 1km

[a] *Calculated from LAStools using average value of ten tiles of lidar data based on all returns.*

Table S2: Environmental predictor variables considered for inclusion in the Random Forest models of post-fire understorey fuel metrics. Variables included in the modelling are indicated in bold; non-bolded variables were excluded due to strong correlation (Pearson r >|0.75|) with one or more bolded variables (as listed in the final column, including the direction of correlation). Values are the mean, minimum and maximum of each predictor for the 1084 lidar plots.

Variable (abbreviation in brackets)	**Units**	**Mean**	**Min**	**Max**	**Correlation**
Mean annual temperature (MAT) [a]	^{0}C	12.3	10.2	13.9	
Temperature annual range (TAR) [a]	^{0}C	21.8	18.6	24.89	
Mean temperature of warmest quarter [a]	^{0}C	17.7	15.7	19.6	MAT (+)
Mean temperature of coldest quarter [a]	^{0}C	6.9	4.4	8.4	MAT (+)
Mean annual precipitation [a]	mm	1199	866	1596	MAT (-)
Precipitation of wettest month [a*]	mm	155	103	229	MAT (-)
Precipitation of driest month [a*]	mm	47	35	57	MAT (-)
Precipitation seasonality (PS, coefficient of variation) [a*]	%	34	22	46	
Precipitation of wettest quarter [a*]	mm	433	285	628	MAT (-)

Precipitation of driest quarter [a*]	mm	176	133	213	MAT (-)
Precipitation of warmest quarter (PWQ) [a*]	mm	180	139	230	
Precipitation of coldest quarter [a*]	mm	431	284	628	MAT (-)
Annual heat moisture index [a]		19.0	12.9	27.2	MAT (+)
Topographic Wetness Index (TWI) [b]		7.00	4.24	15.22	
Elevation [c]	m	539	247.7	1027.6	MAT (-)
Slope [c]	0	16.4	1.5	52.8	
Northness (NTH) [c]		0.15	-0.99	1.00	
Eastness (EST) [c]		-0.08	-1.00	1.00	
Aridity index (AI) [d]		1.62	0.83	2.40	

[a] VicClim data (250-m resolution) by Stewart and Nitschke (2017)

[a*] Precipitation data (250-m resolution) by Fedrigo *et al.* (2019)

[b] TWI (90-m resolution) derived from CSIRO & TERN Soil and Landscape Grid Australia (Gallant and Dowling, 2003)

[c] Estimated from the 5-m lidar-derived DEM based on the 2016 lidar dataset

[d] 20-m resolution (Nyman et al., 2014)

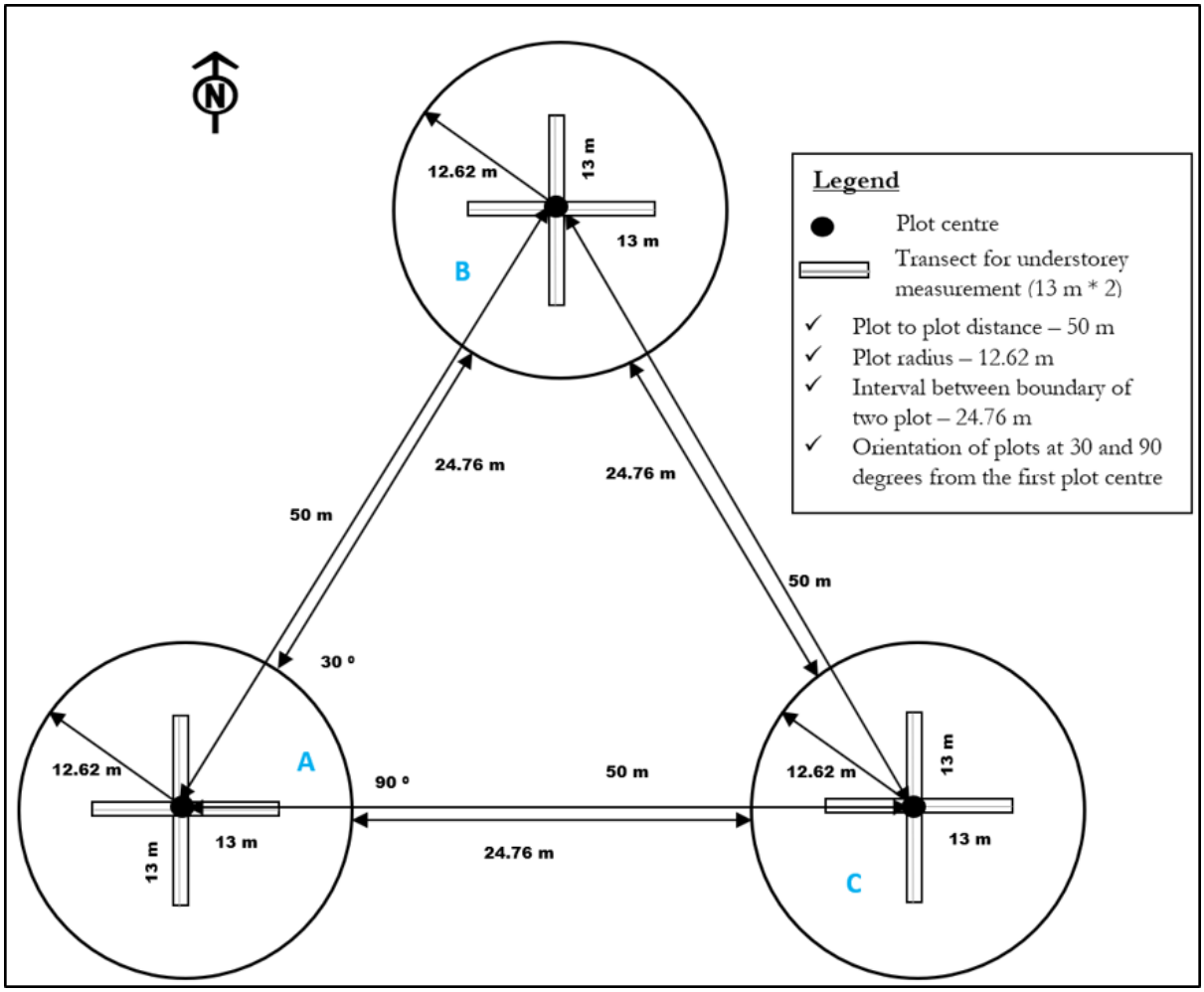

Fig. S1. Sample plot layout for field assessments illustrating the arrangement of three plots per site (minimum distance of 50 m between the plot centres, orientated at 30 and 90 degrees from the centre of plot 'A') and the orientation of two 26 m understorey transects (north-south, east-west) per plot. Figure previously published in Karna et al. (2020).

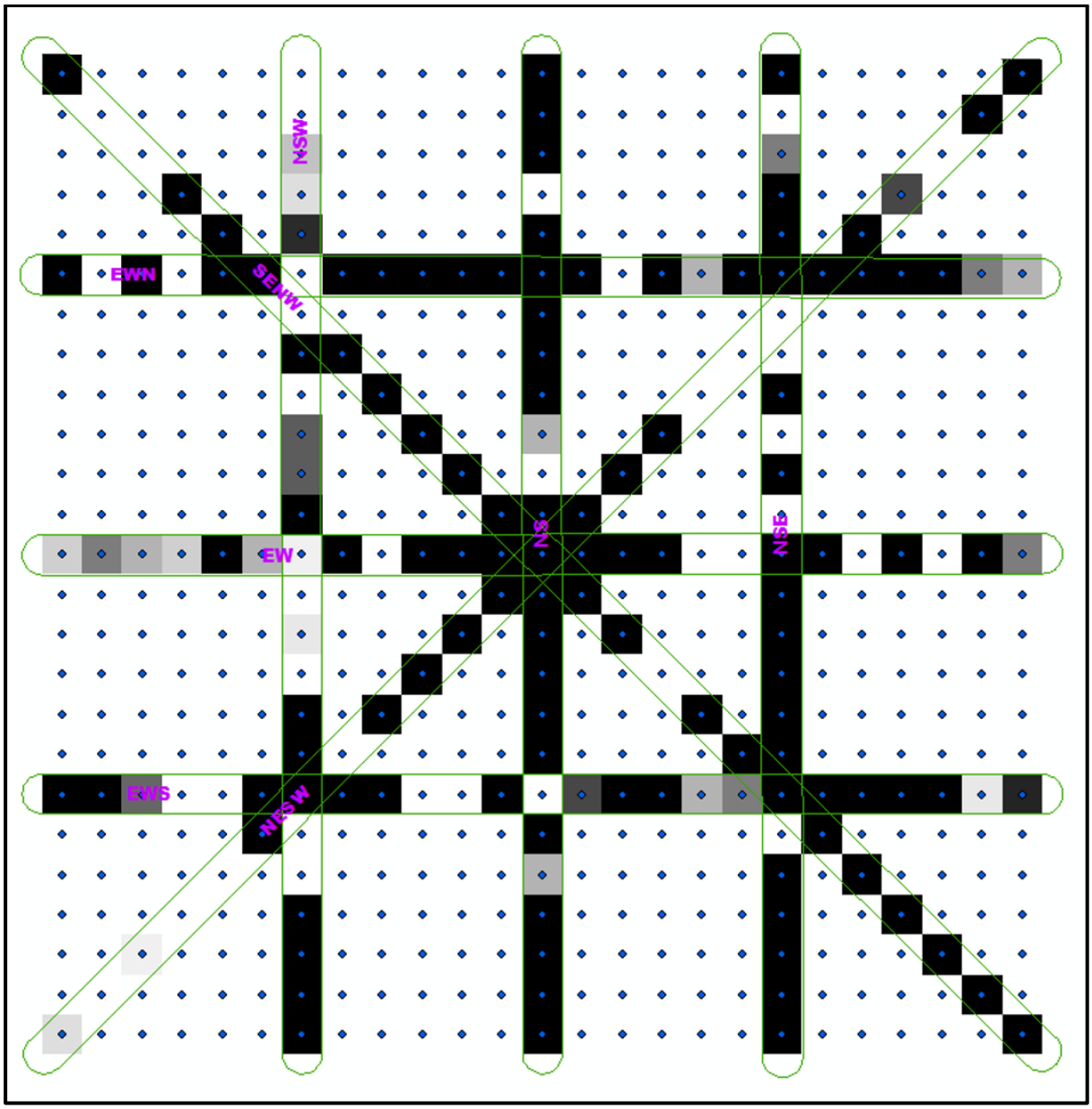

Fig. S2. Rays and raster method illustrating the arrangement of cells in the raster data used to estimate coefficient of variation of understory cover and vertical connectivity metrics in each lidar plot (25 m x 25 m). Measured cells (1 m x 1 m) were in eight 'rays' indicated by green lines (ray name in pink), with cell centers indicated by blue dots. Cell values per metric range from low (white) to high (black) with the scale dependent on the metric being estimated; for example, 0 to 100% for cover values by strata, and 0.15 m to maximum tree height for vertical metrics.

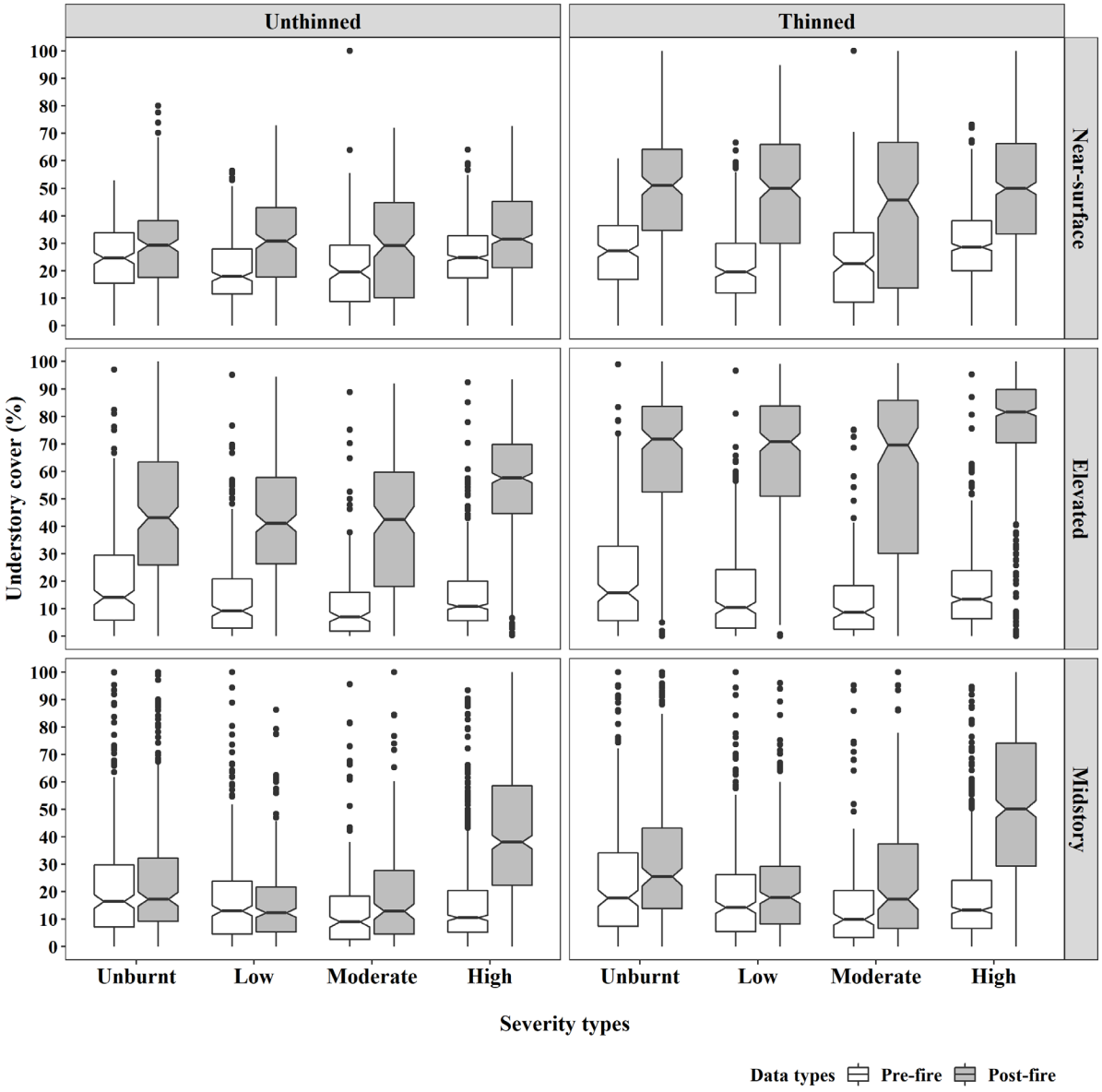

Fig. S3 Boxplots of pre- (2007) and post-fire (2016) understory cover in three strata estimated using the original lidar point densities ('unthinned', left panel) and a down-sampled ('thinned', right panel) point density of 2 m^{-2}, which was close to the original point density of the 2007 data (1.92 m^{-2}). Boxplots indicate the median (as center line), 25th (lower box limit) and 75th (upper box limit) percentiles, and the 95% confidence interval of the median (notches).

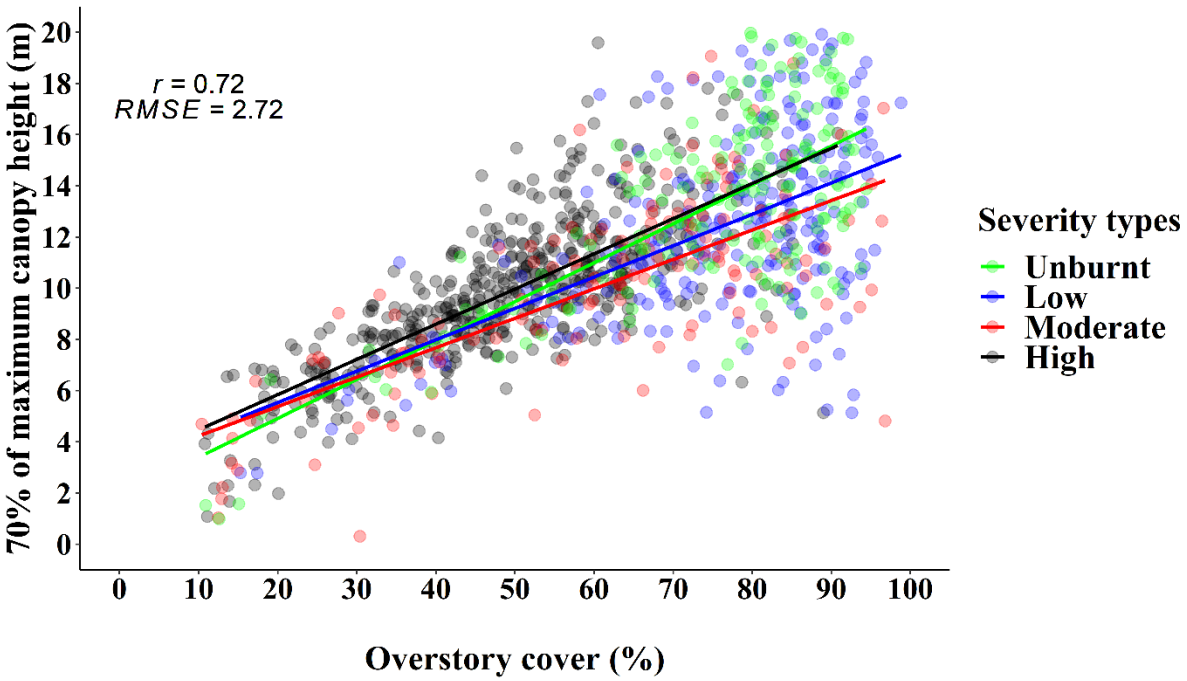

Fig. S4. Relationship between 70% maximum canopy height and overstory cover of different fire-severity types from post-fire lidar data for 1084 random plots of different severity types (unburnt, 198; low-severity, 251, moderate-severity, 138; high-severity, 497). Points and lines with different colours represent different fire severities (Pearson r and RMSE are relevant to the relationship across all fire severities).

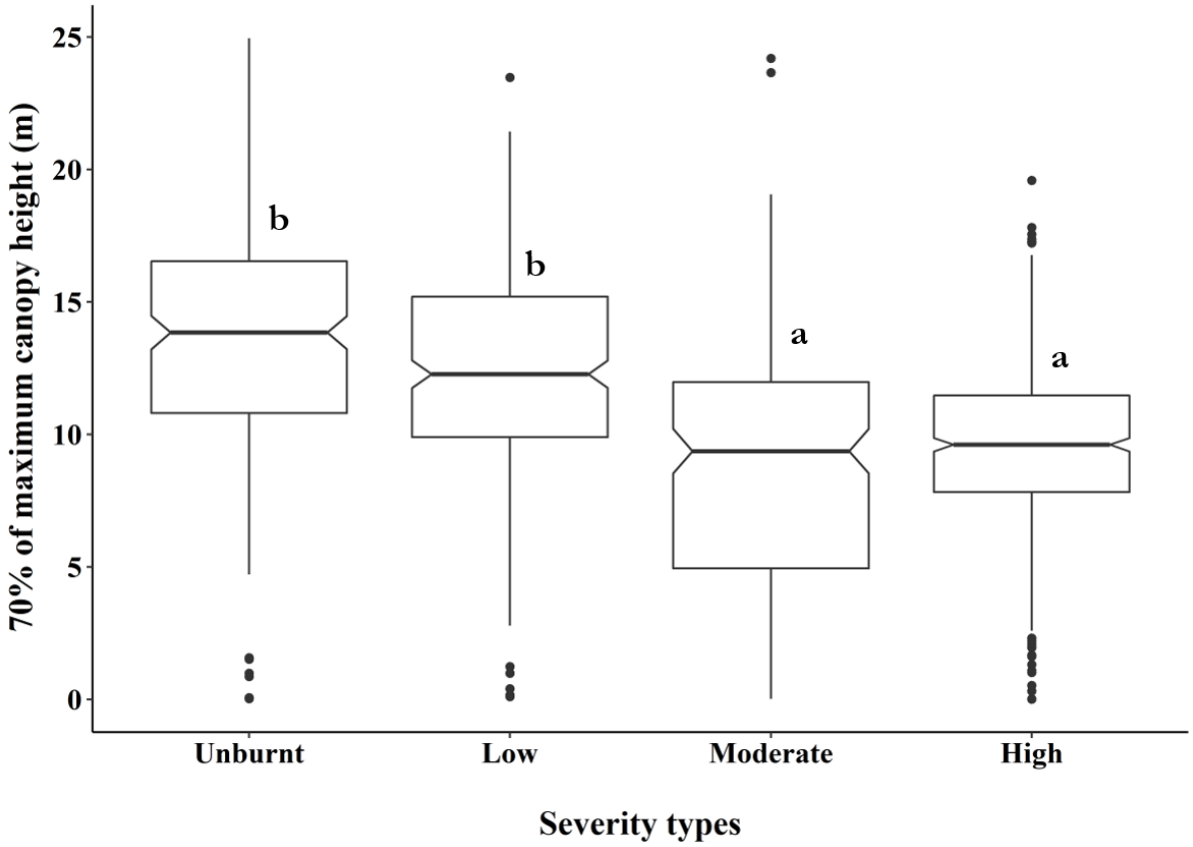

Fig. S5. Boxplots of 70% maximum canopy height of different fire severity types from post-fire lidar data for 1084 random plots of the study area. Boxplots indicate the median (as center line), 25th (lower box limit) and 75th (upper box limit) percentiles, and the 95% confidence interval of the median (notches). Different letters indicate significant differences between fire-severity types (Tukey test; P<0.05) based on adjusted means after an analysis of covariance including the pre-fire '70% of maximum canopy height' as the covariate.

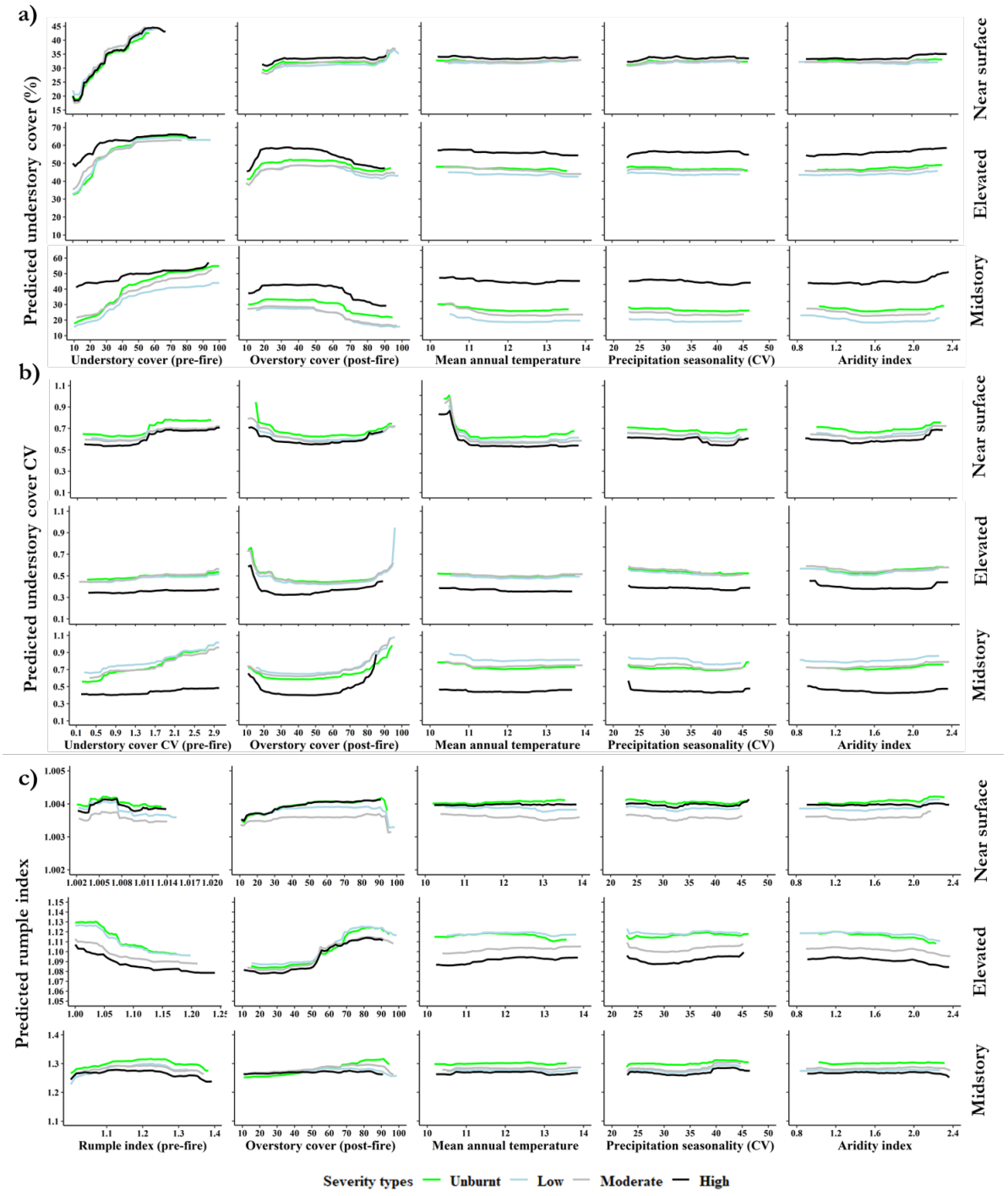

Fig. S6. Partial dependence plots of post-fire lidar horizontal connectivity metrics from Random Forest models for a) understory cover, b) CV of understory cover, and c) rumple index of three understory strata (near surface, elevated and midstory) with selected predictor variables and by fire-severity types. Partial dependence plots indicate the dependency of each understory metric on the predictor after averaging out the effects of all other predictor variables in the model.

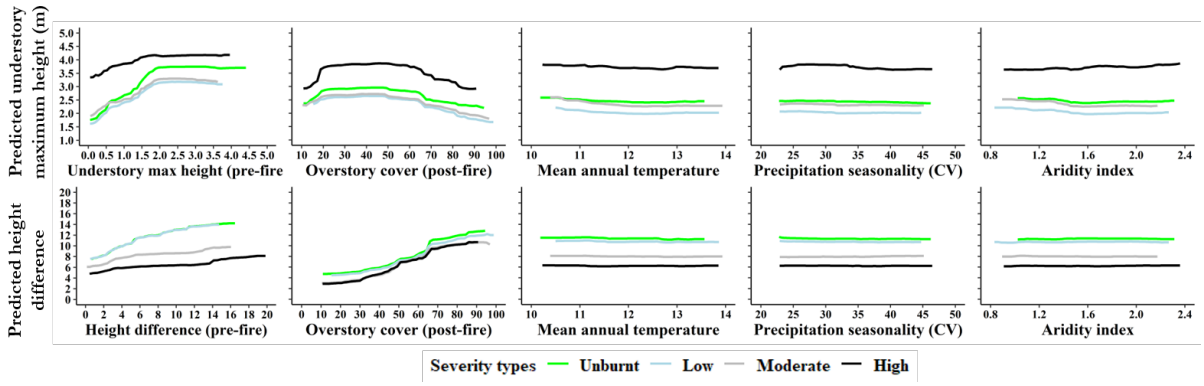

Fig. S7. Partial dependence plots of post-fire lidar vertical connectivity metrics (maximum understory height, and maximum understory and 70% of maximum canopy height difference). Partial dependence plots indicate the dependency of each understory metric on the predictor after averaging out the effects of all other predictor variables in the model.

References:

Fedrigo, M., Stewart, S.B., Roxburgh, S.H., Kasel, S., Bennett, L.T., Vickers, H., Nitschke, C.R., 2019. Predictive Ecosystem Mapping of South-Eastern Australian Temperate Forests Using Lidar-Derived Structural Profiles and Species Distribution Models. Remote Sens. 11, 93.

Gallant, J.C., Dowling, T.I., 2003. A multiresolution index of valley bottom flatness for mapping depositional areas. Water Resources Research 39, n/a-n/a.

Nyman, P., Sherwin, C.B., Langhans, C., Lane, P.N., Sheridan, G.J., 2014. Downscaling regional climate data to calculate the radiative index of dryness in complex terrain. Australian Meteorological and Oceanographic Journal 64, 109-122.

Stewart, S.B., Nitschke, C.R., 2017. Improving temperature interpolation using MODIS LST and local topography: a comparison of methods in south east Australia. International Journal of Climatology 37, 3098-3110.